Short communication

Densitometric, morphometric and mechanical distributions in the human proximal femur

Ara Nazarian[a,c], John Muller[a], David Zurakowski[b], Ralph Müller[c], Brian D. Snyder[a,b,*]

[a]*Orthopedic Biomechanics Laboratory, Beth Israel Deaconess Medical Center, Harvard Medical School, 330 Brookline Avenue, RN115, Boston, MA 02215, USA*
[b]*Department of Orthopaedic Surgery, Children's Hospital, Harvard Medical School, Boston, MA 02115, USA*
[c]*Institute for Biomedical Engineering, University and ETH Zürich, 8044 Zürich, Switzerland*

Abstract

With the prevalent use of DXA-measured BMD to assess pathologic hip fractures and its recently reported lack of reliability to predict fracture or account for efficacy of anti-resorptive therapy, it is reasonable to assess whether variations in the primary and secondary tensile and compressive trabecular microstructure can account for variations in proximal femur strength in comparison to DXA-measured BMD. To that end, microstructural and densitometric measures of trabecular bone specimens, from discrete sites within the proximal femur, were correlated with their mechanical properties. We *hypothesize* that accounting for regional variations in trabecular microstructure will improve predictions of proximal femur strength and stiffness compared to bone density measured by DXA. Forty-seven samples (seven donors) from seven distinct sites of human proximal femur underwent DXA and μCT imaging and mechanical testing. The results revealed significant variations in BMC, morphometric indices and mechanical properties within the proximal femur. This work has demonstrated that the mechanical performance of each sub-region is highly dependent on the corresponding trabecular microstructure. BMD measured by DXA at standard regions of interest cannot resolve the variations in trabecular density and microstructure that govern the mechanical behavior of the proximal femur. This work suggests that a quantitative Singh index that uses high resolution QCT to monitor the trabecular microstructure at specific sub-regions of the proximal femur may allow better predictions of hip fracture risk in individual patients and an improved assessment of changing bone structure in response to pharmacological interventions.

1. Introduction

DXA has been used extensively to measure macroscopic changes in bone mass at the proximal femur that correlate with increased hip fracture risk (Bohr and Schaadt, 1985). However, several longitudinal trials have demonstrated that BMD (g/cm^2) measured at the proximal femur fails to reliably predict fracture occurrence or account for the efficacy of anti-resorptive therapy (Cummings et al., 2002; Riggs and Melton, 2002; Heaney, 2003; Bauer et al., 2004; Schuit et al., 2004). Osteopenic bone diseases affect trabecular architecture and local bone density such that the load bearing capacity of the hip is reduced and the risk for pathologic fracture is increased. According to Wolff's (1892) Law, trabecular morphology of the proximal femur has adapted to optimally support the complex stresses imposed on the hip during stance. The Singh index attempted to correlate the progressive risk for pathologic hip fracture with incremental bone loss from the primary and secondary tensile and compressive trabeculae aligned along the principal stress trajectories of the proximal femur (Singh et al., 1970).

---

*Corresponding author. Orthopedic Biomechanics Laboratory, Beth Israel Deaconess Medical Center, Harvard Medical School, 330 Brookline Avenue, RN115, Boston, MA 02215, USA. Tel.: +1 617 667 2940; fax: +1 617 667 7175.

E-mail addresses: anazaria@bidmc.harvard.edu (A. Nazarian), bsnyder@bidmc.harvard.edu (B.D. Snyder).

However, since the index was subjective and categorical, it could not reliably be used to predict hip fracture risk. Many studies have tested cubes of trabecular bone excised from the proximal femur from multiple donors at a variety of anatomic locations, in an effort to correlate trabecular morphology with mechanical behavior (Brown and Ferguson, 1980). Analytic models have been derived that describe the mechanical properties of trabecular bone as a function of bone density, bone volume fraction (BV/TV), trabecular morphology or a combination of these variables (Carter and Hayes, 1976; Rice et al., 1988; Keller, 1994). While the contribution of trabecular architecture to the overall mechanical behavior of the human proximal femur has been previously explored (Whitehouse and Dyson, 1974; Jayasinghe et al., 1993), few studies have related the variation in trabecular microstructure to the mechanical properties of the proximal femur at specific anatomic sub-regions. To that end, we *hypothesize* that accounting for regional variations in trabecular microstructure will improve predictions of proximal femur strength and stiffness compared to bone density measured by DXA. Therefore, our *aim* is to demonstrate that variations in the microstructure of the primary and secondary tensile and compressive trabeculae account for variations in proximal femur strength and stiffness better than variations in BMD.

2. Methods

Seven fresh frozen cadaveric femurs from seven male, Caucasian donors with no known skeletal pathology were obtained. Seven specimens per proximal femur were cored under copious irrigation across seven identical sites from the proximal femur; two from femoral head, four from femoral neck, and one from the trochanteric region (S1–S7 in Fig. 1), to provide 47 cylindrical cores. The specimens were cored out of pre-cut blocks of femoral bone, with the proper orientation determined from the contact X-ray imaging. The first block was cut at the junction of the femoral head and neck, the second block constituted the femoral neck below the first block, the third block was cut from the trochanteric fossa to the superior aspect of the lesser trochanter, and the last block was cut from the lateral prominence of the greater trochanter to the inferior aspect of the lesser trochanter. The specimens maintained a 2:1 aspect ratio ($\varnothing$: $4.57\,\text{mm} \pm 0.15$, H: $9.85\,\text{mm} \pm 0.80$) with the proper number of open cells to satisfy continuum of material assumptions (Harrigan and Mann, 1984; Gibson and Ashby, 1997). Prior to testing, pre-aligned brass end-caps were glued with cyanoacrylate to the ends of specimens (Fig. 2a) to reduce end artifacts (Keaveny et al., 1997).

Cored specimens underwent X-ray imaging (Faxitron X-ray Systems, McMinnville, OR) to investigate the integrity of the trabecular architecture in each specimen and to discard fractured specimens (two specimens were damaged during preparation and excluded from the study). The mineral content of the specimens was assessed via DXA measurements (PIXImus2, GE Lunar, Madison, WI). The total mineral content (BMC, g) and areal bone mineral density (BMD, g/cm^2) were analyzed by drawing a region of interest enveloping the entire specimen.

Specimens underwent μCT imaging (μCT20, Scanco Medical AG, Bassersdorf, Switzerland) to assess trabecular bone volume fraction and other standard micro-architectural indices in cored specimens. Measurements were stored in three-dimensional image arrays with isotropic voxel sizes of $34\,\mu$m. A three-dimensional Gaussian filter ($\sigma = 1.2$) with a limited, finite filter support (2) was used to suppress the noise in the volumes. These images were binarized to separate bone from background using a global thresholding procedure (Müller and Ruegsegger, 1997a) at
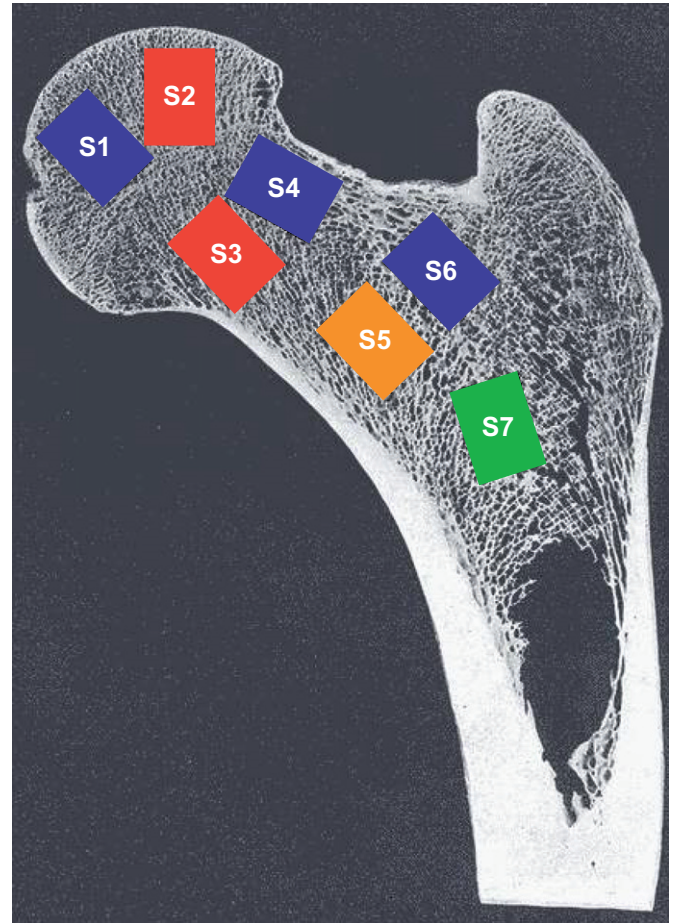

Fig. 1. The layout of the cored specimens (S1–S7) demonstrated on a proximal femur image.

22.4%. To these images, a component labeling algorithm was applied to keep only the largest connected bone-component and to remove small particles arising from noise and artifacts. Bone volume fraction (BV/TV, %), bone surface density (BS/TV, mm^{-1}), trabecular thickness (Tb.Th, mm), trabecular number (Tb.N, mm^{-1}), trabecular separation (Tb.Sp, mm), MIL tensor (H_1, H_2, H_3, mm), degree of anisotropy (DA) and structural model index (SMI) were assessed using distance transformation based direct techniques not relying on a priori assumptions about the underlying structure (Hildebrand et al., 1999; Müller and Ruegsegger, 1997b).

Prior to mechanical testing, pre-aligned brass end caps with a 9 mm diameter and 1.2 mm thickness were glued with cyanoacrylate (American Glue Corp., Taylor, MI) to both ends of the specimens. This step effectively reduced end artifact (Keaveny et al., 1997) by restraining displacement at either end of the specimens and providing support to the free ends of the trabeculae. All specimens underwent previously described compressive mechanical testing (Fig. 2b) using a custom build screw driven mechanical testing system (Nazarian and Müller, 2004; Nazarian et al., 2005). Specimens were preconditioned to eliminate typical toe behavior (Keaveny et al., 1993a, b, 1997; Müller et al., 1998) at a strain rate of $0.005\,\text{s}^{-1}$ for seven cycles and then subjected to monocyclic displacement to failure at a strain rate of $0.01\,\text{s}^{-1}$. The specimens were maintained wet for the duration of mechanical testing, and displacement was measured using a linear variable displacement transducer (LVDT) recording the inter-platen displacement. Relevant parameters such as modulus of elasticity (E), stiffness (K), yield strain (ε_Y) and strength (S_Y) were calculated accordingly.

To account for the repeated-measures of multiple sites for each femur, analysis of variance (ANOVA) using a linear mixed model was applied to test for differences between the seven sites with respect to morphometric,
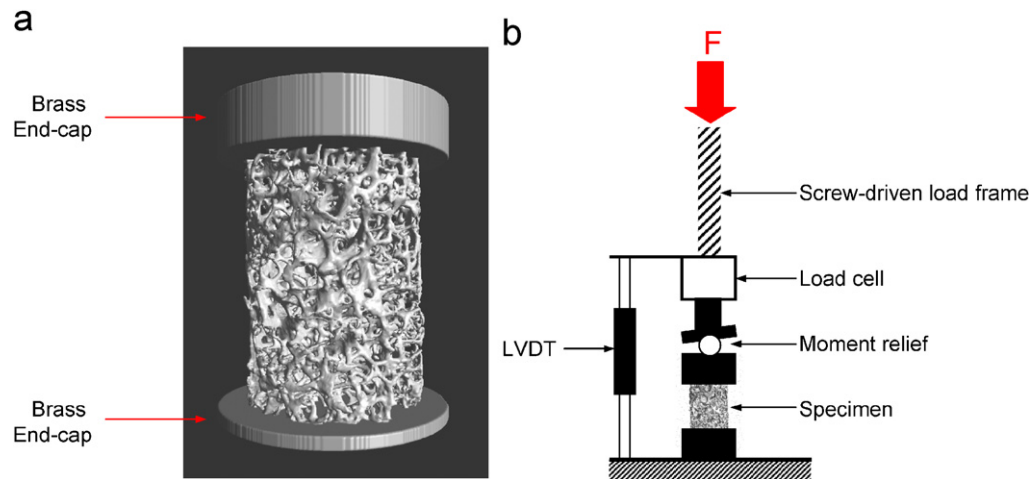
Fig. 2. (a) μCT image of a representative specimen with brass end caps attached at both ends prior to mechanical testing; and (b) a schematic diagram of the mechanical testing system used in the study.

Table 1
Site specific differences in densitometric and mechanical properties[a]

Site	BMD (g/cm^2) Mean (95% CI)	BMC (g) Mean (95% CI)	S_Y (MPa) Mean (95% CI)	E (MPa) Mean (95% CI)
S1	0.08 (0.06–0.10)	0.05 (0.04–0.06)	4.9 (2.0–7.6)	187 (134–239)
S2	0.11 (0.09–0.14)	0.07 (0.06–0.08)	9.1 (6.1–12.1)	329 (274–385)
S3	0.10 (0.08–0.12)	0.06 (0.05–0.07)	6.7 (4.0–9.6)	263 (211–316)
S4	0.09 (0.07–0.11)	0.05 (0.04–0.07)	5.7 (2.7–8.7)	175 (119–231)
S5	0.06 (0.04–0.08)	0.03 (0.02–0.04)	2.9 (0.0–5.9)	137 (81–193)
S6	0.07 (0.05–0.09)	0.04 (0.03–0.05)	4.4 (1.6–7.2)	166 (114–219)
S7	0.06 (0.04–0.08)	0.03 (0.02–0.04)	2.7 (0.0–5.5)	170 (117–222)
CV[b] (%)	37.06	42.45	75.13	35.17
F-test	6.57	7.69	2.38	8.02
p-value	<0.001	<0.001	0.04	<0.001

[a]Site S2 is significantly different compared to sites S5, S6, and S7 for BMD and BMC, and vs. site S7 for S_Y, and vs. sites S1, S4, S5, S6, and S7 for E. CI—confidence interval.
[b]Coefficient of variation.

densitometric and mechanical properties. This approach was chosen to account for the multiple sites per femur and used a compound symmetry covariance structure to model the data (Vittinghoff et al., 2005). Pair wise comparisons between the seven sites were evaluated using a conservative Bonferroni post hoc procedure in order to protect against Type I errors due to multiple comparisons between the sites. The coefficients of variation for all densitometric, morphometric and mechanical parameters were reported for specimens at each site. Additionally, correlation coefficient values (via linear regression) between BMD, BMC, BV/TV, Tb.N, Tb.Th and Tb.Sp and modulus of elasticity and yield strength across all sites were reported. Two-tailed values of $p < 0.05$ were considered significant. SPSS version 14.0 was used for statistical analysis (SPSS Inc., Chicago, IL).

3. Results

Statistical analysis between the seven sites of the proximal femur (between-site distribution) revealed significant differences in BMC ($p < 0.001$) and BMD ($p < 0.001$) (Table 1). Between-site post hoc analysis of the μCT data revealed significant variations in BV/TV, BS/TV, SMI,

Tb.N, Tb.Sp and Tb.Th indices between site 2 and sites 5–7 ($p < 0.05$ for all cases) (Table 2). The MIL tensor vector in the principal direction (H_2) was the only exception, where no between-site variation was observed ($p = 0.07$).

Mechanical testing results suggested that there are significant between-site variations for E ($p < 0.001$), and S_Y ($p = 0.04$) (Table 1, Fig. 4a). Bone mineral content, BMC, BV/TV, E, and S_Y followed similar patterns across all seven sites. Sites S2 and S3 consistently displayed the highest values of density (BMD, BMC, BV/TV) and strength (E and S_Y). Additionally, the same sites consisted of the most plate like trabeculae, with the highest Tb.Th, Tb.N and the lowest Tb.Sp. In contrast, sites S5–S7 reported the opposite densitometric, strength and microstructural patterns than those observed in S2 and S3.

Bone surface density (BS/TV) and Tb.N each explained 77%, Tb.Th 57%, Tb.Sp 70%, and H_2 described 62% of the variation in the modulus of elasticity, respectively. BMC and BV/TV results were highly correlated with each

Table 2
Site specific differences in μCT measured key morphometric indices[a]

Site	BV/TV (%) Mean (95% CI)	Tb.N (1/mm) Mean (95% CI)	Tb.Th (mm) Mean (95% CI)	Tb.Sp (mm) Mean (95% CI)
S1	25.2 (18.1–32.4)	2.0 (1.7–2.3)	0.12 (0.10–0.14)	0.38 (0.22–0.55)
S2	36.0 (28.4–43.6)	2.3 (1.9–2.6)	0.16 (0.14–0.18)	0.28 (0.11–0.46)
S3	30.8 (23.6–37.9)	2.0 (1.7–2.3)	0.15 (0.13–0.17)	0.38 (0.21–0.54)
S4	27.1 (19.5–34.7)	1.8 (1.5–2.1)	0.14 (0.12–0.16)	0.48 (0.30–0.66)
S5	19.0 (11.4–26.6)	1.6 (1.2–1.9)	0.12 (0.10–0.14)	0.56 (0.38–0.73)
S6	20.4 (13.3–27.6)	1.7 (1.4–2.0)	0.12 (0.10–0.14)	0.51 (0.34–0.67)
S7	17.3 (10.1–24.5)	1.5 (1.2–1.8)	0.11 (0.09–0.13)	0.65 (0.49–0.82)
CV[b] (%)	42.40	24.28	23.48	50.31
F-test	5.19	4.12	4.05	2.76
p- value	<0.001	0.003	0.004	0.028

[a]Site S2 is significantly different compared to sites S5, S6, and S7 for BV/TV and Tb.N, and vs. site S7 for Tb.Th and Tb.Sp.
[b]Coefficient of variation.

other ($R^2 = 0.93$); however, BV/TV obtained from μCT imaging described 74% of the variation in modulus of elasticity in contrast to only 65% from DXA measured BMC (Fig. 3a and b) (Fig. 4).

Correlation coefficient values were reported for the six densitometric (BMD and BMC) and morphometric (BV/TV, Tb.N, Tb.Th and Tb.Sp) parameters, obtained from DXA and μCT, versus the modulus of elasticity and yield strength across all sites (Table 3). On average, correlations were higher for yield strength, with all correlations fluctuating between 62% and 82%. All twelve correlations were statistically significant ($p < 0.001$) with trabecular spacing being inversely correlated with modulus of elasticity and yield strength, whereas the other parameters were positively correlated.

Based on the results from this study, human proximal femur exhibits 37% variation in BMD and 42% variation in BMC and BV/TV. Mechanical properties of the proximal femur can vary from 35% in E to 75% in S_Y across all specimens. The variation within the morphometric indices is the highest for SMI (52%) and lowest for DA (14%) (Tables 1, 2 and 4).

4. Discussion

The mechanical properties of the proximal femur have been optimized to accommodate its complex geometry and the forces imposed on it during gait. As postulated by Wolff, the trabecular microstructure reflects the principal stress magnitudes and directions generated during the stance phase of gait. The primary compressive trabeculae form a central pillar of densely packed, plate-like trabeculae ideally suited to support axial compressive loads, while the primary tensile trabeculae form an arc along the femoral neck to resist cantilever-bending moments.

The MIL tensor vector in the principal direction was not significantly different across sites, suggesting that all
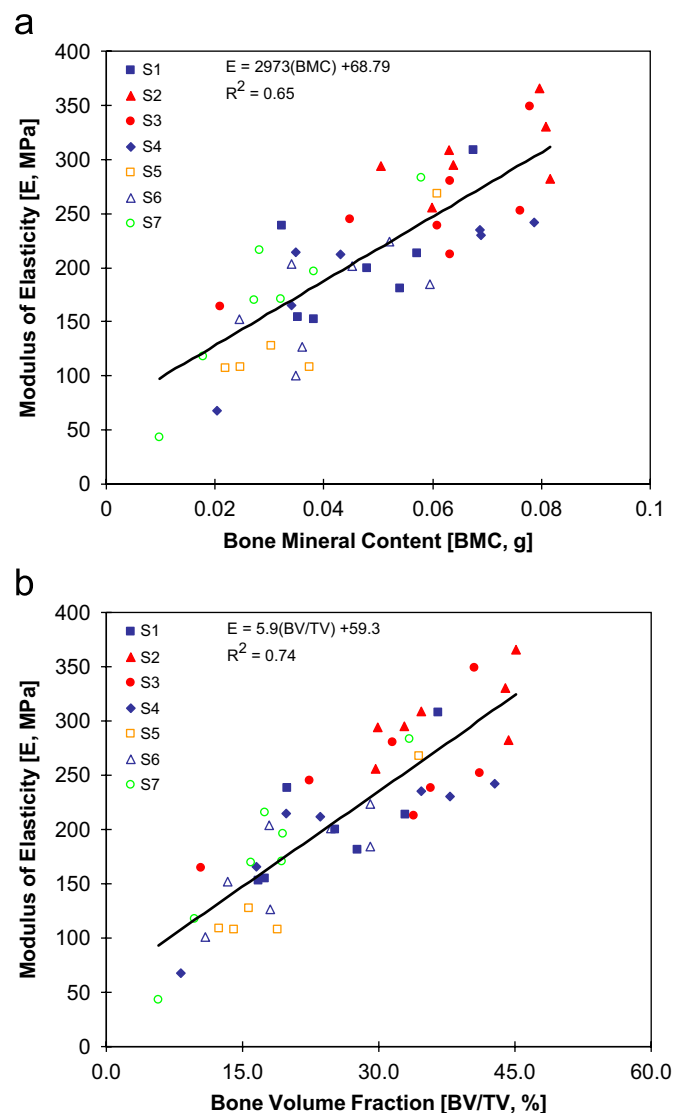

Fig. 3. (a and b) Highlight the relationships between BMC and BV/TV with modulus of elasticity with each site within the proximal femur identified with a separate data point marker.
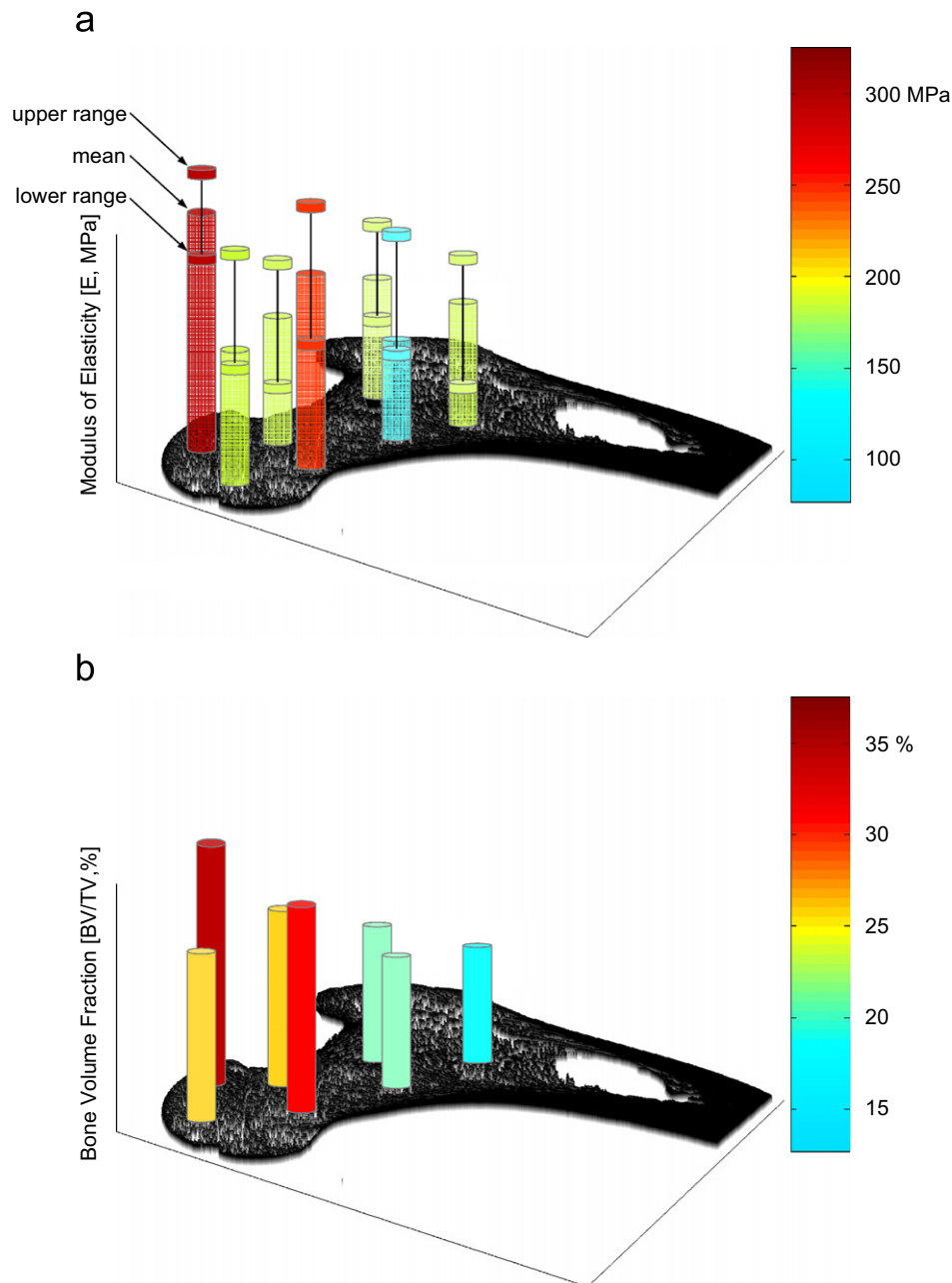
Fig. 4. Three-dimensional visualization of the average (a) Modulus (E) with the upper and lower limits of data at each site; and (b) bone volume fraction (BV/TV) distribution of human proximal femur. In (a), sites S1, S4, S6 and S7 form a loop or belt from the femoral head, through the neck and onto the trochanteric region, where the applied load (in a relatively uniform magnitude) traverses through the proximal femur and disburses into the cortical shaft. It is possible that the loads resultant from normal daily activities are mostly translated though this loop, whereas sites S2 and S3 encounter the higher loads applied to the proximal femur for higher impact activities.

specimens were cored along the principal direction, therefore reducing the possibility of variations in microstructure and strength due to off-axis coring of specimens. The pattern of variation across sites was consistent for all measures of density, microstructure and strength, confirming the close relationships among these parameters and their adaptive responses to exerted forces.

The primary tensile trabeculae are longer and thinner, suitable for resisting the tensile stresses that develop during bending, but if suddenly loaded in axial compression, such as occurs with a fall onto the greater trochanter, the trabeculae will buckle and fracture due to their high slenderness ratio. The decussating arches formed by the secondary tensile and compressive trabeculae at the base of the femoral neck and inter-trochanteric sub-regions are structurally weaker and may explain the propensity for hip fractures at these locations. In osteopenic bone conditions, progressive resorption of the primary compressive trabeculae will increase the risk for pathologic hip fracture during weight bearing.

Table 3
Correlation matrix for densitometric and morphometric parameters versus modulus and strength[a]

Parameter	S_Y (MPa)	E (MPa)
BMD (g/cm^2)	0.82	0.72
BMC (g)	0.82	0.72
BVTV (%)	0.80	0.72
Tb.N (1/mm)	0.67	0.74
Tb.Th (mm)	0.82	0.62
Tb.Sp (mm)	−0.64	−0.70

[a]Values represent Pearson correlation coefficients as obtained from linear regression (all $p < 0.001$).

Table 4
Descriptive statistics for morphometric indices of human proximal femur trabecular bone across all sites

(b)	SMI	DA	H1	H2	H3
Mean	1.13	1.52	0.50	0.77	0.61
Std. dev.	0.58	0.21	0.18	0.28	0.23
CV (%)	51.68	13.92	35.46	37.01	37.84
Min	−0.13	1.12	0.35	0.46	0.41
Max	2.39	2.14	1.33	1.76	1.45

It is important to note that the donor age range and the number of donors/specimens used in this study are limiting factors in assessing microstructural changes due to aging and/or over a wider patient age range, as these issues are outside the scope of this work.

We have demonstrated that the mechanical performance of each sub-region is highly dependent on the corresponding trabecular microstructure. BMD measured by DXA at standard regions of interest cannot resolve the variations in trabecular density and microstructure that govern the mechanical behavior of the proximal femur. This work suggests that a quantitative Singh index that uses high resolution QCT to monitor the trabecular microstructure at specific sub-regions of the proximal femur may allow better predictions of hip fracture risk in individual patients and an improved assessment of changing bone structure in response to pharmacological interventions.

References

Bauer, D.C., et al., 2004. Change in bone turnover and hip, non-spine, and vertebral fracture in alendronate-treated women: the fracture intervention trial. Journal of Bone and Mineral Research 19 (8), 1250–1258.

Bohr, H., Schaadt, O., 1985. Bone mineral content of the femoral neck and shaft: relation between cortical and trabecular bone. Calcified Tissue International 37 (4), 340–344.

Brown, T.D., Ferguson Jr., A.B., 1980. Mechanical property distributions in the cancellous bone of the human proximal femur. Acta Orthopaedica Scandinavica 51 (3), 429–437.

Carter, D.R., Hayes, W.C., 1976. Bone compressive strength: the influence of density and strain rate. Science 194 (4270), 1174–1176.

Cummings, S.R., et al., 2002. Improvement in spine bone density and reduction in risk of vertebral fractures during treatment with antiresorptive drugs. American Journal of Medicine 112 (4), 281–289.

Gibson, L.J., Ashby, M.F., 1997. Cellular Solids, Structure and Properties. Cambridge University Press, Cambridge.

Harrigan, T.P., Mann, R.W., 1984. Characterization of microstructural anisotropy in orthotropic materials using a second rank tensor. Journal of Materials Science 19, 761–767.

Heaney, R.P., 2003. Is the paradigm shifting? Bone 33 (4), 457–465.

Hildebrand, T., Laib, A., Muller, R., Dequeker, J., Ruegsegger, P., 1999. Direct three-dimensional morphometric analysis of human cancellous bone: microstructural data from spine, femur, iliac crest, and calcaneus. Journal of Bone and Mineral Research 14, 1167–1174.

Jayasinghe, J.A., Jones, S.J., Boyde, A., 1993. Scanning electron microscopy of human lumbar vertebral trabecular bone surfaces. Virchows Archiv A—Pathological Anatomy and Histopathology 422 (1), 25–34.

Keaveny, T.M., Borchers, R.E., Gibson, L.J., Hayes, W.C., 1993a. Theoretical analysis of the experimental artifact in trabecular bone compressive modulus. Journal of Biomechanics 26 (4–5), 599–607.

Keaveny, T.M., Borchers, R.E., Gibson, L.J., Hayes, W.C., 1993b. Trabecular bone modulus and strength can depend on specimen geometry. Journal of Biomechanics 26 (8), 991–1000.

Keaveny, T.M., Pinilla, T.P., Crawford, R.P., Kopperdahl, D.L., Lou, A., 1997. Systematic and random errors in compression testing of trabecular bone. Journal of Orthopaedic Research 15 (1), 101–110.

Keller, T.S., 1994. Predicting the compressive mechanical behavior of bone. Journal of Biomechanics 27 (9), 1159–1168.

Müller, R., Ruegsegger, P., 1997a. Micro-tomographic imaging for the nondestructive evaluation of trabecular bone architecture. Studies in Health Technology and Information 40, 61–79.

Müller, R., Ruegsegger, P., 1997b. Micro-tomographic imaging for the nondestructive evaluation of trabecular bone architecture. Studies in Health Technology and Information 40, 61–79.

Müller, R., Gerber, S.C., Hayes, W.C., 1998. Micro-compression: a novel technique for the nondestructive assessment of local bone failure. Technology and Health Care 6 (5–6), 433–444.

Nazarian, A., Müller, R., 2004. Time-lapsed microstructural imaging of bone failure behavior. Journal of Biomechanics 37 (1), 55–65.

Nazarian, A., Stauber, M., Müller, R., 2005. Design and implementation of a novel mechanical testing system for cellular solids. Journal of Biomedical Materials Research B—Applied Biomaterials 73 (2), 400–411.

Rice, J.C., Cowin, S.C., Bowman, J.A., 1988. On the dependence of the elasticity and strength of cancellous bone on apparent density. Journal of Biomechanics 21 (2), 155–168.

Riggs, B.L., Melton 3rd, L.J., 2002. Bone turnover matters: the raloxifene treatment paradox of dramatic decreases in vertebral fractures without commensurate increases in bone density. Journal of Bone and Mineral Research 17 (1), 11–14.

Schuit, S.C., et al., 2004. Fracture incidence and association with bone mineral density in elderly men and women: the Rotterdam study. Bone 34 (1), 195–202.

Singh, M., Nagrath, A., Maini, P., 1970. Changes in trabecular pattern of the upper end of the femur as an index of osteoporosis. Journal of Bone and Joint Surgery 52-A, 457–467.

Vittinghoff, E., Glidden, D.V., Shiboski, S.C., McCulloch, C.E., 2005. Regression Methods in Biostatistics. Linear, Logistic, Survival, and Repeated Measures Models. Springer, New York.

Whitehouse, W.J., Dyson, E.D., 1974. Scanning electron microscope studies of trabecular bone in the proximal end of the human femur. Journal of Anatomy 118 (Pt 3), 417–444.

Wolff, J., 1892. Das Gesetz der Transformation der Knochen (The Law of Bone Remodelling). Springer, Berlin, Germany.